

Pairing, Charge, and Spin Correlations in the Three-Band Hubbard Model

Z. B. Huang and H. Q. Lin *

Department of Physics, Chinese University of Hong Kong, Hong Kong, China

J. E. Gubernatis

Theoretical Division, Los Alamos National Laboratory, Los Alamos, NM 87545

(October 31, 2018)

Using the Constrained Path Monte Carlo (CPMC) method, we simulated the two-dimensional, three-band Hubbard model to study pairing, charge, and spin correlations as a function of electron and hole doping and the Coulomb repulsion V_{pd} between charges on neighboring Cu and O lattice sites. As a function of distance, both the $d_{x^2-y^2}$ -wave and extended s-wave pairing correlations decayed quickly. In the charge-transfer regime, increasing V_{pd} decreased the long-range part of the correlation functions in both channels, while in the mixed-valent regime, it increased the long-range part of the s-wave behavior but decreased that of the d-wave behavior. Still the d-wave behavior dominated. At a given doping, increasing V_{pd} increased the spin-spin correlations in the charge-transfer regime but decreased them in the mixed-valent regime. Also increasing V_{pd} suppressed the charge-charge correlations between neighboring Cu and O sites. Electron and hole doping away from half-filling was accompanied by a rapid suppression of anti-ferromagnetic correlations.

I. INTRODUCTION

In this paper, we will report the results of a quantum Monte Carlo (QMC) study of the ground-state properties of the two-dimensional, three-band Hubbard model. Of the three simple electronic models commonly studied as possible models of the cuprate superconducting materials, the three-band Hubbard model has been the least intensively studied, partially because of the general belief that its low energy excitation spectrum is similar to the other two. Indeed in the strong coupling limit, both the one-band and three-band Hubbard models have the t-J model as an approximate limit. However, there still remains some controversy about whether one-band models, like the Hubbard and t-J models, are adequate to describe the low energy physical properties of the cuprate superconductors. One of our objectives was to study the possible existence of superconductivity in the three-band model in regions where model parameters are physical as opposed to regions where asymptotic models are clearly

more appropriate. A focus of our ground state study is the effect of the inclusion of V_{pd} , a repulsive Coulomb interaction between charges on neighboring Cu and O lattice sites.

The most solid information about possible superconductivity in the one-band Hubbard model has come from a series of QMC calculations. For instance, using a finite temperature QMC method, White et al.¹ found an attractive effective pairing interaction in the $d_{x^2-y^2}$ and extended s-wave channels. Moreo and Scalapino² subsequently found pairing correlations but also found that they did not increase when the lattice size was increased. This result, suggesting the absence of off-diagonal long range order, was consistent with an earlier QMC study by Imada and Hatsugai.³

The fermion sign problem limits almost all QMC calculations of the Hubbard model to small system sizes and finite temperature simulations to high temperatures. These limitations had left open the possibility that superconductivity still lurked at larger systems sizes and lower temperatures. Recently, a new zero temperature QMC method, the Constrained Path Monte Carlo (CPMC) method,⁴ was developed to get around the sign problem. Using this method, Zhang et al.⁵ calculated ground-state pairing correlation functions for the Hubbard model as a function of the distance and found that as the system size or the interaction strength is increased the magnitude of the long-range part of the pairing correlation functions vanished for both the $d_{x^2-y^2}$ and extended s-wave channels. Although this method produces an approximate solution, its results, together with the null results from previous QMC studies, are very discouraging for finding superconductivity in the one-band Hubbard model.

At finite temperature, past numerical work on the three-band model has included several sets of QMC simulations,⁶⁻¹¹ focusing on the magnetic superconducting and insulating properties of the model. As for the QMC simulations of the Hubbard model, the sign problem limited these studies to relatively high temperatures and small systems. In fact the sign problem for the three-band model is probably more severe than for the one band model. At least the one band model lacks a sign problem at half filling. In general, an anti-ferromagnetic state is found at half-filling which is strongly suppressed upon doping. Attractive interactions between pairs were found with a spectrum of results: Dominance of extended s-wave and d-wave pairing have been separately

*Corresponding author, email address: hqlin@phy.cuhk.edu.hk

reported, leading to claims of extended s-wave and d-wave ODLRO. These results remain controversial.

At zero temperature, past numerical work on the three-band model has mainly consisted of exact diagonalization computations,^{12–14} where calculations of hole binding energies was emphasized, and several QMC computations^{16,15,17} where pairing calculations were emphasized. The exact diagonalization studies unequivocally established that holes can bind. The QMC studies, established the existence of an extended s-wave and $d_{x^2-y^2}$ wave attractive pairing interaction, with one claim of of no evidence of s-wave superconductivity. More recently, a CPMC study by Guerrero and Gubernatis¹⁸ confirmed the exact diagonalization result that holes bind but found that increasing system size tended to decrease the long range part of the pairing correlations. In contrast to the exact diagonalization work, this QMC study found hole binding in the absence of a Coulomb repulsion V_{pd} between charge on neighboring Cu and O sites. The exact diagonalization studies found that hole binding required an unphysically large value of V_{pd} .

In the work reported here, we applied the CPMC method to the three-band Hubbard model and computed the static pairing, charge, and spin correlation functions for systems with 6×6 unit cells. We set the hopping and on-site Coulomb parameters as expected physically relevant values and studied the properties of the systems as a function of charge-transfer energy, electron and hole doping, and V_{pd} through a range of physically relevant values. The consequences of varying these parameters for the most part depended on whether the value of the charge-transfer energy placed the model in a charge-transfer or mixed valent regime. The cuprate superconductors are believed to be in the charge-transfer regime.

The remainder of our report is organized as follows: In Section II, we define the Hamiltonian and the physical quantities calculated and discuss the choice of model parameters. In Section III we briefly describe the CPMC method, and then in Section IV, we present our numerical results. Finally in Section V, we discuss in detail our main conclusions.

II. THREE-BAND HUBBARD HAMILTONIAN

As proposed by Emery,¹⁹ the three-band model mimics the CuO_2 layer in the cuprate superconductors by having one Cu and two O atoms per unit cell, with the Cu atoms arranged on a square lattice and the O atoms centered on the edges of the square unit cells. In this layer, Emery assumed that the relevant orbitals are just those of copper $3d_{x^2-y^2}$ and oxygen $2p_x$ and $2p_y$.

The Hamiltonian has the form:

$$H = \sum_{\langle j,k \rangle \sigma} t_{pp}^{jk} (p_{j\sigma}^\dagger p_{k\sigma} + p_{k\sigma}^\dagger p_{j\sigma}) + \epsilon_p \sum_{j\sigma} n_{j\sigma}^p + U_p \sum_j n_{j\uparrow}^p n_{j\downarrow}^p + \epsilon_d \sum_{i\sigma} n_{i\sigma}^d + U_d \sum_i n_{i\uparrow}^d n_{i\downarrow}^d \quad (1)$$

$$+ V_{pd} \sum_{\langle i,j \rangle} n_i^d n_j^p + \sum_{\langle i,j \rangle \sigma} t_{pd}^{ij} (d_{i\sigma}^\dagger p_{j\sigma} + p_{j\sigma}^\dagger d_{i\sigma})$$

In writing the Hamiltonian, we adopted the convention that the operator $d_{i\sigma}^\dagger$ creates a *hole* with spin σ at a Cu $3d_{x^2-y^2}$ orbital and $p_{j\sigma}^\dagger$ creates a *hole* with spin σ in an O $2p_x$ or $2p_y$ orbital. U_d and U_p are the Coulomb repulsions at the Cu and O sites, ϵ_d and ϵ_p are the corresponding orbital energies, and V_{pd} is the nearest neighbor Coulomb repulsion. As written, the model has a Cu-O hybridization $t_{pd}^{ij} = \pm t_{pd}$ with the minus sign occurring for $j = i + \hat{x}/2$ and $j = i - \hat{y}/2$ and also hybridization $t_{pp}^{jk} = \pm t_{pp}$ between oxygen sites with the minus sign occurring for $k = j - \hat{x}/2 - \hat{y}/2$ and $k = j + \hat{x}/2 + \hat{y}/2$. These phase conventions are illustrated in Fig. 1.

The values of the parameters in the Hamiltonian have been estimated by a number of different constrained density functional and quantum cluster calculations.^{20–24} In electron-volts reasonable ranges for these values seem to be: $t_{pd} = 1.3 - 1.6$, $U_d = 8.5 - 10.5$, $\epsilon = \epsilon_p - \epsilon_d = 3.6$, $U_p = 4.0 - 7.5$, $t_{pp} = 0.65$, and $V_{pd} = 0.6 - 1.2$. Taken together, these estimates define a reasonably limited range of the parameters for the which the model might be labeled as “physical.”

The Cu site Coulomb repulsion U_d is a large energy, making doubly occupancy of Cu sites by two holes very unfavorable. The next largest parameter, the charge transfer energy $\epsilon = \epsilon_p - \epsilon_d > 0$, plays a special role. Dependent on the relative values of ϵ , U_d and the bandwidth W , the system can be classified in different regimes:²⁵ the charge-transfer regime with $U_d > \epsilon > W$ or the mixed-valent regime with $U_d > W > \epsilon$, where W is some measure of the width of the lower band. Estimates place the cuprate superconductors in the charge-transfer regime. The role of the Cu-O hybridization t_{pd} is important. Through the super-exchange mechanism, this hybridization generates an antiferromagnetic exchange interaction between the spins in the Cu sites. The O-O hybridization t_{pp} and the O site Coulomb repulsion U_p are the two smallest energies. When t_{pp} is non-zero, the non-interacting band structure has features that seem to appear in the normal state properties of the cuprate materials. We were mainly interested in studying the consequences of V_{pd} . These consequences were studied in part by previous QMC simulations of Dopf et al.⁹ and Scalettar et al.⁷ In what follows we will scale all the energies by t_{pd} .

For the non-interacting case ($U_p = U_p = V_{pd} = 0$), the band structure is easily determined numerically and is illustrated in Fig. 2 for a set of parameters used. We will add and remove holes from lower band, and this band is said to be half-filled when there is one hole per unit cell. At half-filling, for a wide range of parameters, the ground-state is an anti-ferromagnetic insulator just like the one-band Hubbard model. This band gap can be estimated from Fig. 2. A better physical feel can be obtained from the exact expression easily obtained if $t_{pp} = 0$: It is simply ϵ . The band-width $W = \sqrt{(\epsilon/2)^2 + 8} - \epsilon/2$. It

varies monotonically from 8 to zero as ϵ varies from zero to infinity. $\epsilon = 2$ marks a value for which $W = \epsilon$. This picture does not change much for relatively small non-zero values of t_{pp} . As shown by Dopf et al.⁹, for $\epsilon = 1$ the charge transfer gap is vanishing small, whereas for $\epsilon = 3$ a finite charge transfer gap arises in the strong-coupling region. $\epsilon = 1$ is in the mixed valent regime, while $\epsilon = 3$ is in the charge transfer regime. And we will see that $\epsilon = 2$ behaves more like the charge-transfer than the mixed-valent regime. In Fig. 3, we show the Fermi surfaces for infinite systems at the various dopings studied.

If $\epsilon \gg U_d$, the three-band model maps into a one-band model with $t_{eff} \sim t_{pd}^2/\epsilon$ and $U = U_d$. For $U_d \gg t_{eff}$, the one-band model can in turn be mapped into the t-J model with $J = 4t_{eff}^2/U_d$. Zhang and Rice²³ have argued that the t-J model can also be appropriate when $0 < t_{pd} \ll \epsilon, U_d, U_d - \epsilon$. In real materials, ϵ/t_{pd} is estimated to be $\sim 2.7 - 3.7$.²⁴ Therefore, besides the lack of conclusive evidence that the one-band model superconducts, it is also unclear that the mapping among the most studied models is appropriate for physical values of the parameters.

With the numerical method used, a variety of expectation values can be computed. We focused on the pairing, spin, and charge correlation functions. More specifically we computed the extended s-wave and the $d_{x^2-y^2}$ pairing correlations as functions of distance

$$P_\alpha(\vec{R}) = \langle \Delta_\alpha^\dagger(\vec{R}) \Delta_\alpha(0) \rangle \quad (2)$$

where

$$\begin{aligned} \Delta_\alpha(\vec{R}) = \sum_{\vec{\delta}} f_\alpha(\vec{\delta}) \{ & [d_{\vec{R}\uparrow} d_{\vec{R}+\vec{\delta}\downarrow} - d_{\vec{R}\downarrow} d_{\vec{R}+\vec{\delta}\uparrow}] \\ & + [p_{\vec{R}\uparrow}^x p_{\vec{R}+\vec{\delta}\downarrow}^x - p_{\vec{R}\downarrow}^x p_{\vec{R}+\vec{\delta}\uparrow}^x] \\ & + [p_{\vec{R}\uparrow}^y p_{\vec{R}+\vec{\delta}\downarrow}^y - p_{\vec{R}\downarrow}^y p_{\vec{R}+\vec{\delta}\uparrow}^y] \} \end{aligned}$$

with $\vec{\delta} = \pm\hat{x}, \pm\hat{y}$. For the extended s-wave pairing $f_{s^*}(\vec{\delta}) = 1$ for all $\vec{\delta}$ and for the $d_{x^2-y^2}$ pairing, $f_d(\vec{\delta}) = 1$ for $\vec{\delta} = \pm\hat{x}$ and $f_d(\vec{\delta}) = -1$ for $\vec{\delta} = \pm\hat{y}$. The magnitude of these quantities are dominated by a large peak in $P_\alpha(\vec{R})$ when $R = |\vec{R}|$ is less than a few nearest neighbor distances. Over these distances, P_α measures local correlations among spin and charge, has little information about long-range pairing correlations, and may give a “false positive” indication of enhanced pairing. Because of this we will report neither the $q = 0$ spatial Fourier transformation nor the partial sums like $S_\alpha(L) = \sum_{R \leq L} P_\alpha(\vec{R})$ as done in some previous works.⁶⁻¹⁶ Instead we will report $S_\alpha(L) = \sum_{R \geq L} P_\alpha(\vec{R})$ where L is about two lattice spacings. We will also report the “vertex contribution” to the correlation functions (see, for example, White et al.¹) defined as follows:

$$V_\alpha(\vec{R}) = P_\alpha(\vec{R}) - \bar{P}_\alpha(\vec{R}), \quad (3)$$

where $\bar{P}_\alpha(\vec{R})$ is the contribution of dressed non-interacting propagator: for each term in $P_\alpha(\vec{R})$ of the form $\langle c_\uparrow^\dagger c_\uparrow c_\downarrow^\dagger c_\downarrow \rangle$, $\bar{P}_\alpha(\vec{R})$ has a term like $\langle c_\uparrow^\dagger c_\uparrow \rangle \langle c_\downarrow^\dagger c_\downarrow \rangle$. We found that in most cases the conclusions remain the same no matter which quantity we look at.

For the static spin-spin correlation function we used the Fourier transform of the spin-spin correlation function for the spin on the Cu sites

$$S(k) = \frac{1}{N} \sum_{lm} e^{ik \cdot (l-m)} \langle (n_{l,\uparrow}^d - n_{l,\downarrow}^d)(n_{l+m,\uparrow}^d - n_{l+m,\downarrow}^d) \rangle, \quad (4)$$

where l and m refers to the Cu sites and N is the number of unit cells. For charge-charge correlations we computed a charge-transfer correlation function involving the O sites neighboring a Cu site quantity:

$$C(k) = \frac{1}{N} \sum_{ij} e^{ik \cdot (i-j)} \langle \rho(i) \rho(j) \rangle. \quad (5)$$

where j are the nearest-neighbors of i , $\rho(i) = n_i^d - n_i^{p_x} - n_i^{p_y}$ with n_i^d , $n_i^{p_x}$, and $n_i^{p_y}$ being the charge-density operators on the Cu, x-axis O, and y-axis O in the unit cell i .

III. NUMERICAL METHOD

Our numerical method, the constrained path Monte Carlo (CPMC) method, is extensively described and benchmarked elsewhere^{4,5}. Here we only discuss its basic strategy and approximation. In the CPMC method, the ground-state wave function $|\psi_0\rangle$ is projected from a known initial wave function $|\psi_T\rangle$ by a branching random walk in an over-complete space of Slater determinants $|\phi\rangle$. In such a space, we can write $|\psi_0\rangle = \sum_\phi \chi(\phi) |\phi\rangle$. The random walk produces an ensemble of $|\phi\rangle$, called random walkers, which represent $|\psi_0\rangle$ in the sense that their distribution is a Monte Carlo sampling of $\chi(\phi)$, that is, a sampling of the ground-state wave function. More specifically, starting with some trial state $|\psi_T\rangle$, we project out the ground state by iterating

$$|\psi'\rangle = e^{-\Delta\tau(H-E_T)} |\psi\rangle \quad (6)$$

where E_T is some guess of the ground-state energy. Purposely $\Delta\tau$ is a small parameter so for $H = T + V$ we can write

$$e^{-\Delta\tau H} \approx e^{-\Delta\tau T/2} e^{-\Delta\tau V} e^{-\Delta\tau T/2} \quad (7)$$

where T and V are the kinetic and potential energies.

For the study at hand, the initial state $|\psi_T\rangle$ is the direct product of two spin Slater determinants, i.e.,

$$|\psi_T\rangle = \prod_\sigma |\phi_\sigma^\sigma\rangle \quad (8)$$

Because the kinetic energy is a quadratic form in the creation and destruction operators for each spin, the action of its exponential on the trial state is simply to transform one direct product of Slater determinants into another. While the potential energy is not a quadratic form in the creation and destruction operators, its exponential is replaced by sum of exponentials of such forms via the discrete Hubbard-Stratonovich transformation. For the on-site Coulomb term, this transformation is

$$e^{-\Delta\tau U_d n_{i,\sigma}^d n_{i,-\sigma}^d} = \frac{1}{2} \sum_{x=\pm 1} e^{-x\Delta\tau J_d (n_{i,\sigma}^d - n_{i,-\sigma}^d)} e^{\frac{1}{2}\Delta\tau U_d (n_{i,\sigma}^d + n_{i,-\sigma}^d)} \quad (9)$$

provided $U_d \geq 0$ and $\cosh \Delta\tau J_d = e^{-\Delta\tau U_d/2}$. For the nearest neighbor Coulomb repulsion term, we make the same type of transformation but we have to do it many more times: $n_{i\uparrow}^d n_{j\uparrow}^d = n_{i\uparrow}^d n_{j\uparrow}^d + n_{i\uparrow}^d n_{j\downarrow}^d + n_{i\downarrow}^d n_{j\uparrow}^d + n_{i\downarrow}^d n_{j\downarrow}^d$. For each term and each j in the \hat{x} and \hat{y} directions, a Hubbard-Stratonovich transformation is required for a total of 8 such transformations. Because the computational time scales with the number of Hubbard-Stratonovich transformations, having a $V_{pd} \neq 0$ increases the computational cost by a factor of 8.

One consequence of the Hubbard-Stratonovich transformation is the factorization of the projection into an up and down spin part. Accordingly we re-express the iteration step as

$$\prod_{\sigma} |\phi'_{\sigma}\rangle = \int d\vec{x} P(\vec{x}) \prod_{\sigma} B_{\sigma}(\vec{x}) |\phi_{\sigma}\rangle \quad (10)$$

where $\vec{x} = (x_1, x_2, \dots, x_N)$ is the set of Hubbard-Stratonovich fields (one for each lattice site), N is the number of lattice sites, $P(\vec{x}) = (\frac{1}{2})^N$ is the probability distribution for these fields, and $B_{\sigma}(\vec{x})$ is an operator function of these fields formed from the product of the exponentials of the kinetic and potential energies.

The Monte Carlo method is used to perform the multi-dimensional integration over the Hubbard-Stratonovich fields. It does so by generating a set of random walkers initialized by replicating $|\psi_T\rangle$ many times. Each walker is then propagated independently by sampling a \vec{x} from $P(\vec{x})$ and propagating it with $B(\vec{x})$. After the propagation has “equilibrated,” the sum over the walkers provides an estimate of the ground-state wave function $|\psi_0\rangle$.

We used two different estimators for the expectation values of some observable \mathcal{O} . One is the mixed estimator

$$\langle \mathcal{O} \rangle_{\text{mixed}} = \frac{\langle \psi_T | \mathcal{O} | \psi_0 \rangle}{\langle \psi_T | \psi_0 \rangle} \quad (11)$$

and the other is the back-propagated estimator

$$\langle \mathcal{O} \rangle_{\text{bp}} = \frac{\langle \psi_T | e^{-\ell\Delta\tau H} \mathcal{O} | \psi_0 \rangle}{\langle \psi_T | e^{-\ell\Delta\tau H} | \psi_0 \rangle} \quad (12)$$

where $|\psi_0\rangle$ is the QMC estimate of the ground state and ℓ is typically in the range of 20 to 40. For observables

that commute with the Hamiltonian, the mixed estimator is a very accurate one and converges to the exact answer as $|\psi_0\rangle$ converges to exact ground state. For observables that do not commute with the Hamiltonian, like correlation functions, the back-propagated estimator has been found to give very accurate estimates of ground-state properties. Significant differences between the predictions of these two estimators often exist.

To completely specify the ground-state wave function for a system of interacting electrons, only determinants satisfying $\langle \psi_0 | \phi \rangle > 0$ are needed because $|\psi_0\rangle$ resides in either of two degenerate halves of the Slater determinant space, separated by a nodal surface \mathbf{N} that is defined by $\langle \psi_0 | \phi \rangle = 0$. The degeneracy is a consequence of both $|\psi_0\rangle$ and $-|\psi_0\rangle$ satisfying Schrödinger’s equation. The sign problem occurs because walkers can cross \mathbf{N} as their orbitals evolve continuously in the random walk. Asymptotically they populate the two halves equally, leading to an ensemble that has zero overlap with $|\psi_0\rangle$. If \mathbf{N} were known, we would simply constrain the random walk to one half of the space and obtain an exact solution of Schrödinger’s equation. In the constrained-path QMC method, without *a priori* knowledge of \mathbf{N} , we use a trial wave function $|\psi_T\rangle$ and require $\langle \psi_T | \phi \rangle > 0$. This is what is called the constrained-path approximation.

All the calculations reported here were done for copper-oxide planes with periodic boundary conditions. Mostly, we study closed shell cases, for which the corresponding free-electron wave function is non-degenerate and translationally invariant. For 6×6 unit cells, the dopings, producing Fermi surfaces in Fig. 2, correspond to closed shell fillings. In these cases, the free-electron wave function, represented by a single Slater determinant, is used as the trial wave function $|\psi_T\rangle$. The use of an unrestricted Hartree-Fock wave function as $|\psi_T\rangle$ generally produced no significant improvement in the results. At half-filling, which is not a closed shell case, we used a linear combination of two degenerate $\mathbf{Q} = (\pi, \pi)$ spin-density wave states.

In a typical run, the average number of walkers was 600, and the time step was 0.03. We performed 1600 steps before we started taking measurements, and we did the measurements in 30 blocks of 320 steps each to ensure statistical independence. Back propagation measurements had 40 backward steps.

IV. RESULTS

As mentioned before, all our simulations were done on lattices of 6×6 unit cells. For this size, 36 holes corresponds to a half-filled case. In units of t_{pd} , we set $U_d = 6$, $U_p = 0$, and $t_{pp} = 0.3$ for most studied cases. We varied V_{pd} between 0 and 1 for several different hole fillings and values of the charge-transfer energy ϵ . We were mainly concerned with hole doped cases. number of holes.

A. Charge Correlation Functions

In Fig. 4 we show the expectation values of the charge on the Cu sites as a function of V_{pd} for several band fillings and values of the charge-transfer energy ϵ . When $V_{pd} = 0$, we see that for the half-filled case, even with a relatively large value of ϵ , there are substantial holes distributed on the O sites. When doped to 42 and 46 holes, most of the added holes go to the O site. Except for the $\epsilon = 1$ case, increasing V_{pd} from 0 transfers some of the O charge to the Cu. The transfer rate increases if ϵ is increased. These are expected results: in the charge-transfer regime, $U_d > \epsilon > W$, with a repulsive V_{pd} , it become energetically favorable for some charge to move from O to Cu even at the expense of some unfavorable double occupancy of the Cu site caused by a large U_d . On the other hand, in the mixed-valent regime, $U_d > W > \epsilon$, when $\epsilon = 1$, we see a movement of holes from the Cu site to the O sites. Here the energy difference between the Cu and O states is smaller, and a strong on-site repulsive U_d favoring charge removable from the Cu sites dominates the smaller repulsive V_{pd} , opposing the movement of charge to the O sites. In general, the presence of V_{pd} seems to expand the charge-transfer regime. Similar results have been seen in finite-temperature QMC⁹ and zero-temperature exact diagonalization⁷ studies.

Another effect of increasing V_{pd} is the decreasing of the correlation between the charge on the Cu and the neighboring O sites. This is shown in Fig. 5. At a given band filling, increasing ϵ only has a little effect. Similar behavior was also seen in a finite-temperature QMC study. One also observes that in the charge-transfer regime the decreasing rate seems independent of the filling and ϵ . Because $C(0) \approx N_h/N - \langle n_{Cu}n_O \rangle$, it is no surprise to observe an increase in $C(\mathbf{k} = 0)$ with an increasing V_{pd} .

It is instructive to compare our findings with Stephan et al.'s¹⁴ results. Their exact diagonalization results showed that when $U_{Cu} = U_O = \infty$, doped holes make the hole on the Cu sites transfer to the O sites, and with increasing V_{pd} , the charge on the Cu site decreases continuously. They also found that the addition of a second hole produces a smaller additional change in the neighboring Cu-O charge correlation than the first one does. Both behaviors of the hole on the Cu site and neighboring Cu-O charge correlation indicate that a charge-transfer ‘‘bipolaron’’ forms in this system. Therefore they concluded that the binding energy is obtained from electronic polarization. From our simulation results, in the charge transfer region, the charge on the Cu site increases with hole doping and increasing V_{pd} , suggesting that electronic polarization has no effect in the physically relevant region. Hence we expect that the binding energy is mainly gained from magnetic mechanism.

B. Spin Correlation Functions

In Fig. 6 we show the behavior of the local magnetic moment on the Cu sites. First, we see that increasing the hole doping increases the moment. More specifically, at a given doping, increasing ϵ increases the moment. When $\epsilon > 1$, increasing V_{pd} increases the moment, but when $\epsilon = 1$, increasing V_{pd} decreases it. Clearly, the increase of the moment is strongly correlated with the increase and decrease of charges on the Cu sites.

In Figs. 7 and 8 we show the wavevector dependence of the Fourier transform of the static spin-spin correlation function for the Cu sites as a function of V_{pd} for a doping to 42 holes. This function is plotted along high symmetry lines in the first Brillouin zone. The different figures corresponds to different values of ϵ . In mixed valent regime, Fig. 7, we see that increasing V_{pd} suppress this function over the entire zone. This suppression is consistent with the suppression of the local moment seen in Fig. 6. On the other hand, in the charge-transfer regime, Fig. 8, increasing V_{pd} enhances this function, again consistent with the enhancement of the local moment seen in Fig. 6. By comparing the two figures we see that for a given V_{pd} increasing ϵ increases these correlations and sharpens the peaks in the functions. In each figure there are two principal peaks: One is connected with the displacement of the antiferromagnetic peak to $(\pi, \pi - \delta)$. The other is the appearance of an incommensurate structure at $(\pi - \delta', \pi - \delta')$. A weaker spin-density wave structure is at $(\pi, 0)$.

Previous QMC simulations of the one-band Hubbard model^{26,27} have seen a similar shifting (and splitting) of the peak in the static structure factor from the antiferromagnetic position (π, π) to positions $(\pi, \pi - \delta)$ on the face of the Brillouin zone and $(\pi - \delta', \pi - \delta')$ along the diagonal direction. This behavior is in agreement with the experimental data for LSCO presented in Fig. 3 of Ref.²⁸, where a minimum is observed at (π, π) along the diagonal direction. Our CPMC simulations of $t - t' - U$ Hubbard model also found that for a large t' , a weak peak appears along the diagonal direction. We remark that we did not study the dependence of either of these peaks on lattice size.

To examine whether the incommensurate peak along the diagonal direction is produced by a finite O-O hopping t_{pp} , in Fig. 9 (a) and (b) we display the spin structure factor $S(k)$ as a function of t_{pp} for different ϵ . The parameters are the same as in Fig. 7. Here a nonzero t_{pp} makes the hole filling correspond to a closed-shell case. From Fig. 9 (b), even for a very small t_{pp} , a weak peak at the $(\pi - \delta', \pi - \delta')$ still exists. With increasing t_{pp} , the spin-spin correlations are strongly suppressed near the AF wavevector (π, π) , and at the same time the amplitude of the incommensurate peak along the diagonal direction or tendency to this peak forming is enhanced. For the half-filling case (data not shown) we also observed that increasing t_{pp} greatly suppresses AF order.

Finally, we report how the AF long range order in the half-filling case is destroyed by the hole doping. In Fig. 10(a) and (b), the spin structure factor is plotted for different hole filling cases. From Fig. 10(a), it is clearly seen that AF spin-spin correlation is strongly suppressed by the hole doping. As shown in Fig. 10(b), in the light hole doping region ($N_h = 42$), there exist two incommensurate peaks. When the system is doped to $N_h = 46$, the incommensurate peak along the diagonal direction disappears, but the peak on the face of the Brillouin zone is robust. In the heavy doping region ($N_h = 54$), the spin structure factor is featureless near (π, π) , and the peak occurs at $(\pi, 0)$.

C. Pairing Correlation Functions

A typical pairing correlation function as a function of distance and V_{pd} is shown in Fig. 11. Here we show the d-wave function and see that it is dominated by a large peak at short distances ($R < 2$). At these distances, increasing V_{pd} increases the magnitudes of the correlations slightly. At larger distances ($R > 2$), the trend reverses. The dominance of the local peak is such that a measure of pairing like the $\mathbf{k} = 0$ dependence of the Fourier transform of the pairing correlation function or the integral of $P(R)$ with a large distance cut-off can exhibit behavior indicative of the only the short-range behavior and hide the more relevant long-range behavior.

The short-range behavior is illustrated in more detail in Fig. 12. For two different values of U_d , we plot the value of the $R = 0$ peak in the vertex contribution for both extended s-wave and d-wave symmetries for several values of ϵ . In both the charge-transfer and mixed valent regimes, the $R = 0$ value for both symmetries increases monotonically with increasing V_{pd} .

For comparison, the long-range ($R > 2$) behavior is illustrated in Fig. 13. In both the s and d-wave channels, the long-range vertex contributions in the charge-transfer regime decrease with increasing V_{pd} but in the mixed-valent regime it increases. Over the range of V_{pd} simulated, the long-range part of the d-wave contribution is consistently larger than the s-wave contribution.

As a function of filling, the behavior is more complex. In Fig. 14 is the short-range part of the vertex contribution. In the mixed valent regime, both the extended s-wave and d-wave channels decrease rapidly with electron and hole doping. In the charge-transfer regime, the d-wave functions falls with doping but the extended s-wave contribution initially increases. The long-range contribution, shown in Fig 15, shows the dominance of the d-wave channel. In the mixed-valent regime it basically decreases with doping, whereas in the charge-transfer regime, it initially increases but only to decrease rapidly for large hole doping. Our findings suggest that the conclusions of Dopf et al.⁹ reflect the behavior of local interaction vertex, not the long range property.

V. SUMMARY AND CONCLUSIONS

We summarize our results as follows: Using the CPMC method, we simulated the two-dimensional three-band Hubbard model to study its charge, spin, and pairing correlations as a function of electron and hole doping, and the charge-transfer energy ϵ and the Coulomb repulsion V_{pd} between charges on neighboring Cu and O lattice sites. We found that increasing V_{pd} suppressed the charge-charge correlations between neighboring Cu and O sites. In the mixed-valent regime it had the effect moving small amounts of charge from the Cu sites to the O sites. In the charge-transfer regime, the effect was the opposite. Upon hole doping, more of the extra holes went to the O sites than to the Cu sites.

At a given doping, increasing V_{pd} increased the spin-spin correlations in the charge-transfer regime but decreased them in the mixed-valent regime. Also electron and hole doping away from half-filling was accompanied by a rapid suppression of anti-ferromagnetic correlations. As a function of doping, ϵ , and V_{pd} , the behavior of the magnetic moment on the Cu sites was strongly correlated with the behavior of the charge on the Cu sites.

As a function of distance, both the $d_{x^2-y^2}$ -wave and extended s-wave pairing correlations decayed quickly. In the charge-transfer regime, increasing V_{pd} decreased the long-range part of the correlation functions in both channels, while in the mixed-valent regime, it increased the long-range part of the s-wave behavior but decreased that of the d-wave behavior decreased. Still the d-wave behavior dominated. At a given doping, increasing V_{pd} increased the spin-spin correlations in the charge-transfer regime but decreased them in the mixed-valent regime. Also electron and hole doping away from half-filling was accompanied by a rapid suppression of anti-ferromagnetic correlations.

We presented a more extensive study of the effects of V_{pd} than previous QMC studies at zero and finite temperature. Our results illustrate the presence of both s and d-wave correlations in the charge-transfer regime, with the d-wave correlations generally dominating. These results highlight the difference in the behavior between the short and long range part of these correlation function. Figures of merits that include the short-range part are dominated by the behavior of the short-range part. For the system size studied the correlations are weak. We did not study these correlations as function of system size. We believe the size dependence will be the same as previous studies.

Lastly, as a complementary part to results presented so far, we briefly report the effects of U_p on charge, magnetic and pairing correlations. In both the mixed valent and charge-transfer regions, and for all band fillings, we found that a finite U_p ($U_p = 2.0$) moves some charge from the oxygen sites to the copper sites, which causes an increasing of magnetic moment at the copper sites. Consistent with previous observations^{13,18} that U_p has a

negative effect on the hole binding, the long-range part of the d-wave correlation functions is suppressed by U_p . Our simulation results also show that U_p has a larger effect in the mixed valent region than that in the charge-transfer region.

ACKNOWLEDGMENTS

The work of Z. B. H. was supported in part by the Earmarked Grant for Research from the Research Grants Council (RGC) of the HKSAR under Projects CUHK 4190/97P-2160089. The work of J. E. G. was supported by the US Department of Energy. Part of his work was performed while as a guest of the Chinese University of Hong Kong. He gratefully acknowledges this hospitality.

-
- ¹ S. R. White, D. J. Scalapino, R. L. Sugar, N. E. Bickers, R. T. Scalettar, Phys. Rev. B, **39**, 839 (1989).
² A. Moreo and D. J. Scalapino, Phys. Rev. B **43**, 8211 (1991).
³ Masatoshi Imada and Yasuhiro Hatsugai, J. Phys. Soc. Jpn., **58**, 3752 (1989).
⁴ Shiwei Zhang, J. Carlson and J. E. Gubernatis, Phys. Rev. Lett., **74**, 3652 (1995); Phys. Rev. B **55**, 7464 (1997); J. Carlson, J. E. Gubernatis, G. Ortiz, and Shiwei Zhang, Phys. Rev. B **59**, 12788 (1999).
⁵ Shiwei Zhang, J. Carlson and J. E. Gubernatis, Phys. Rev. Lett., **78**, 4486 (1997).
⁶ R. T. Scalettar, Physica C, **162-164**, 313 (1989).
⁷ R. T. Scalettar, D. J. Scalapino, R. L. Sugar, S. R. White, Phys. Rev. B **44**, 770 (1991).
⁸ G. Dopf, A. Muramatsu, and W. Hanke, Phys. Rev. B **41**, 9264 (1990).
⁹ G. Dopf, A. Muramatsu, and W. Hanke, Phys. Rev. Lett. **68**, 353 (1992).
¹⁰ G. Dopf, J. Wagner, P. Dieterich, A. Muramatsu, and W. Hanke, Helv. Phys. Acta **65**, 257 (1992).
¹¹ G. Dopf, A. Muramatsu, and W. Hanke, Europhys. Lett. **17**, 559 (1992).
¹² Masao Ogata and Hiroyuki Shiba, J. Phys. Soc. Jpn., **57**, 3074 (1988).
¹³ J. E. Hirsch, S. Tang, E. Loh Jr., D. J. Scalapino, Phys. Rev. Lett. **60**, 1668 (1988); Phys. Rev. B **39**, 243 (1989).
¹⁴ W. H. Stephan, W. v. d. Linden and P. Horsch, Phys. Rev. B **39**, 2924 (1989).
¹⁵ M. Frick, P. C. Pattnaik, I. Morgenstern, D. M. Newns, and W. v. d. Linden Phys. Rev. B **42**, 2665 (1990).
¹⁶ Kazuhiko Kuroki and Hideo Aoki, Phys. Rev. Lett. **76**, 4400 (1996).
¹⁷ See also, H. Endres, W. Hanke, H. G. Evertz, and F. F. Assaad, Phys. Rev. Lett. **78**, 160 (1997); Kazuhiko Kuroki and Hideo Aoki, Phys. Rev. Lett. **78**, 161 (1997).

- ¹⁸ M. Guerrero, J. E. Gubernatis, and Shiwei Zhang, Phys. Rev. B **57**, 11980 (1998).
¹⁹ V. J. Emery, Phys. Rev. Lett. **58**, 2794 (1987).
²⁰ M. S. Hybertsen, M. Schuluter and N. E. Christensen, Phys. Rev. B **39**, 9028 (1989).
²¹ H. Eskes, G. A. Sawatzky, L. F. Feiner, Physica C **160**, 424 (1989).
²² A. K. McMahan, J. F. Annett and R. M. Martin, Phys. Rev. B **42**, 6268 (1990).
²³ F. C. Zhang and T. M. Rice, Phys. Rev. B **37**, 3795 (1988).
²⁴ Richard L. Martin, Phys. Rev. B **53**, 15501 (1996).
²⁵ J. Zaanen and A. M. Oleś, Phys. Rev. B **37**, 9423 (1988).
²⁶ Daniel Duffy and Adriana Moreo, Phys. Rev. B **52**, 15607 (1995).
²⁷ Charles Buhler and Adriana Moreo, Phys. Rev. B **59**, 9882 (1999).
²⁸ T. E. Mason, G. Aeppli, S. M. Haydeu, A. P. Hamiver, and H. A. Mook, Phys. Rev. Lett. **71**, 919 (1993).

FIG. 1. Phase convention for the hopping matrix elements. The copper $d_{x^2-y^2}$ orbital is surrounded by the oxygen p_x and p_y orbitals. The hopping matrix elements are shown with their corresponding phase.

FIG. 2. The band-structure of an infinite systems for $\epsilon = 3$ and $t_{pp}/t_{pd} = 0.3$.

FIG. 3. Fermi surfaces of an infinite-system for $\epsilon = 3$ and $t_{pp}/t_{pd} = 0.3$. From the inside out, the hole fillings are 54/36, 46/36, 42/36, 36/36 (dashed line), and 26/36.

FIG. 4. Average charge on Cu sites as a function of V_{pd} for different fillings and charge-transfer energies ϵ .

FIG. 5. Charge correlation between neighboring Cu and O sites as a function of V_{pd} for different fillings and charge-transfer energies ϵ .

FIG. 6. Average magnetic moment at the Cu sites as a function of V_{pd} for different fillings and charge-transfer energies ϵ .

FIG. 7. Average static spin structure factor for Cu sites as a function of the wavevector \mathbf{k} and V_{pd} . $\epsilon = 1$ and the number of holes equals 42.

FIG. 8. Average static spin structure factor for Cu sites as a function of the wavevector \mathbf{k} and V_{pd} . $\epsilon = 3$ and the number of holes equals 42.

FIG. 9. Average static spin structure factor for Cu sites as a function of the wavevector \mathbf{k} and t_{pp} . (a) $\epsilon = 1$, (b) $\epsilon = 3$, and the number of holes equals 42.

FIG. 10. Average static spin structure factor for Cu sites as a function of the wavevector \mathbf{k} and N_h with $\epsilon = 3$. (a) Half-filling and doped cases and (b) Doped cases.

FIG. 11. d-wave pairing correlation function as a function of distance R for different values of V_{pd} . The number of holes equals 42.

FIG. 12. Local ($R = 0$) vertex contributions to the extended s and d-wave pairing correlation function as a function of V_{pd} for different values of ϵ and V_{pd} . The number of holes equals 42.

FIG. 13. Long-range (averaged for $R > 2$) part of the vertex contributions (averaged over $R > 2$) to the extended s and d-wave pairing correlation function as a function of V_{pd} for different values of ϵ and V_{pd} . The number of holes equals 42.

FIG. 14. Local part ($R = 0$) of the vertex contributions to the extended s and d-wave pairing correlation function as a function of filling. $V_{pd} = 0$. The number of holes equals 42. (a) $\epsilon = 1$. (b) $\epsilon = 3$.

FIG. 15. Long-range part (averaged for $R > 2$) of the vertex contributions to the extended s and d-wave pairing correlation function as a function of filling. $V_{pd} = 0$. The number of holes equals 42. (a) $\epsilon = 1$. (b) $\epsilon = 3$.

figure1

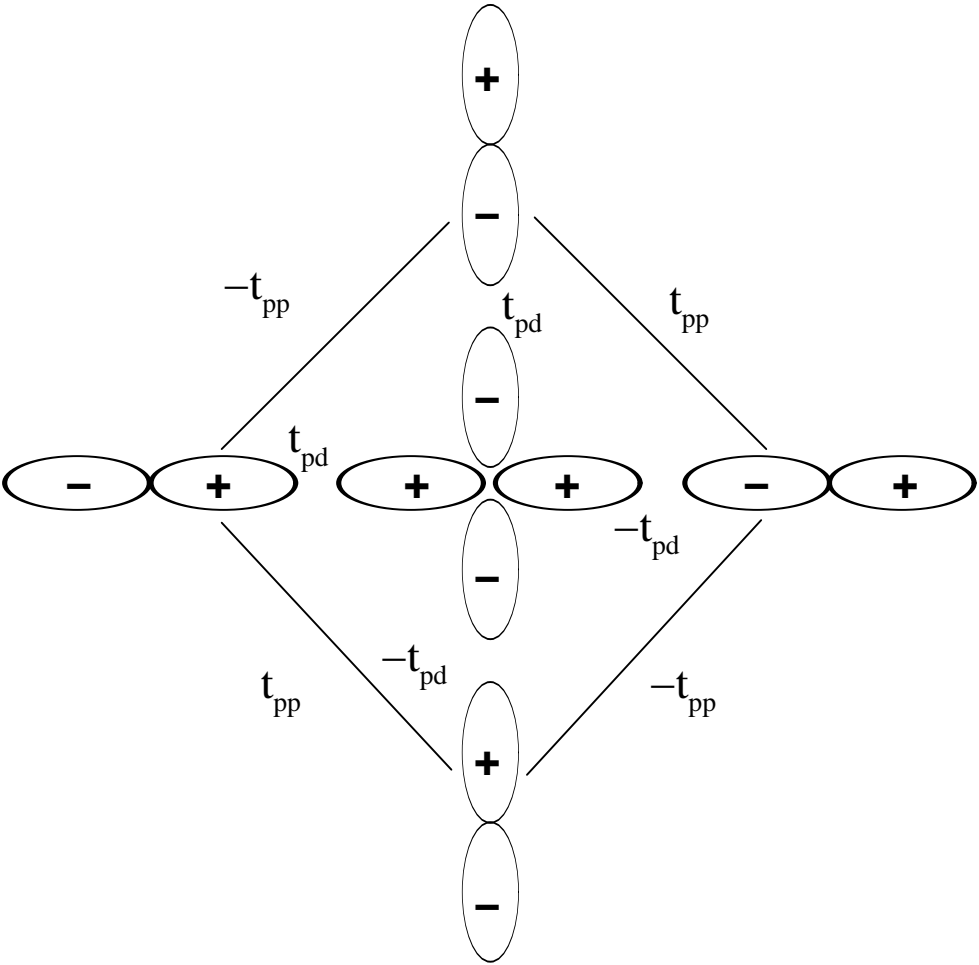


figure2

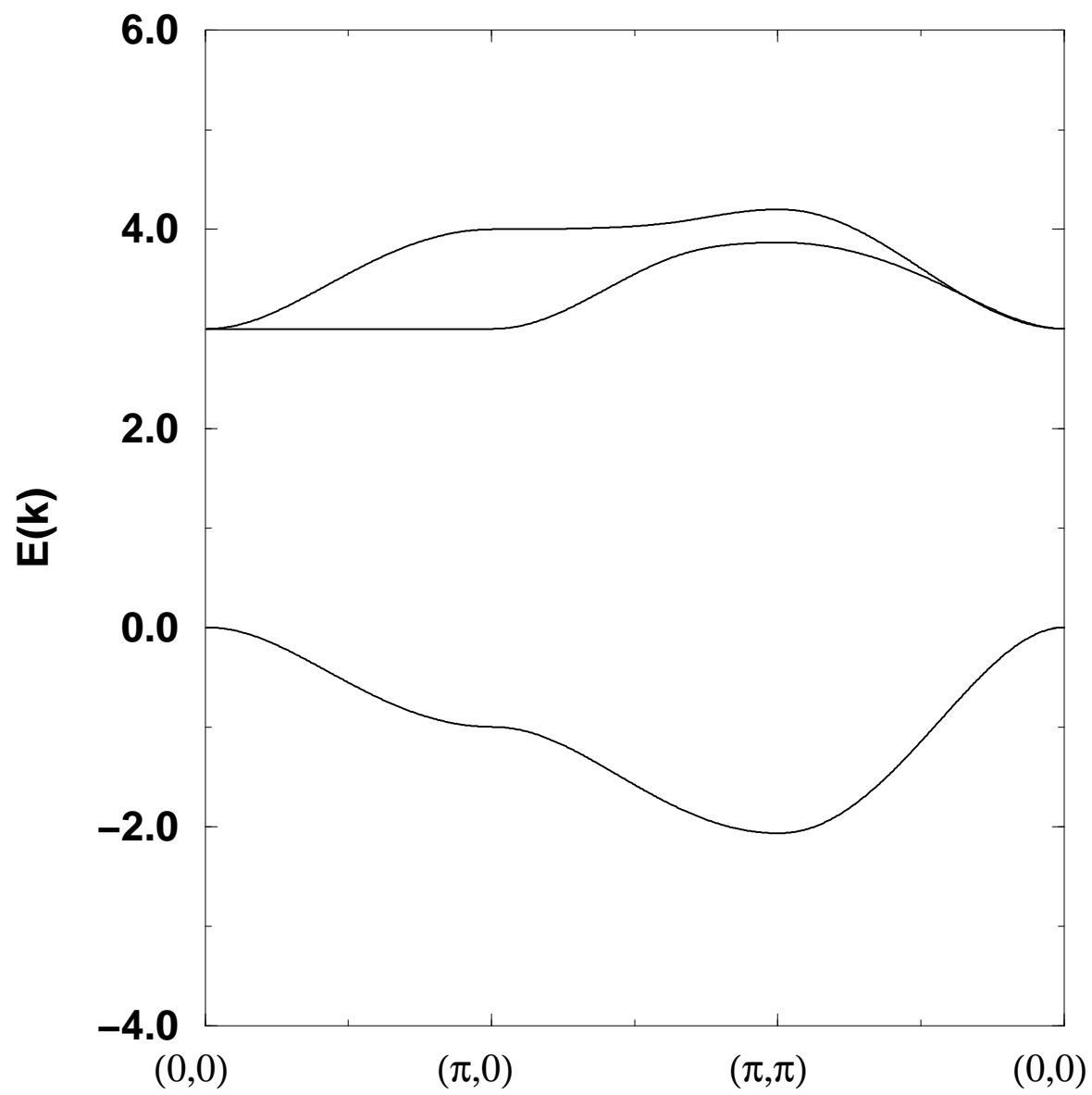


figure3

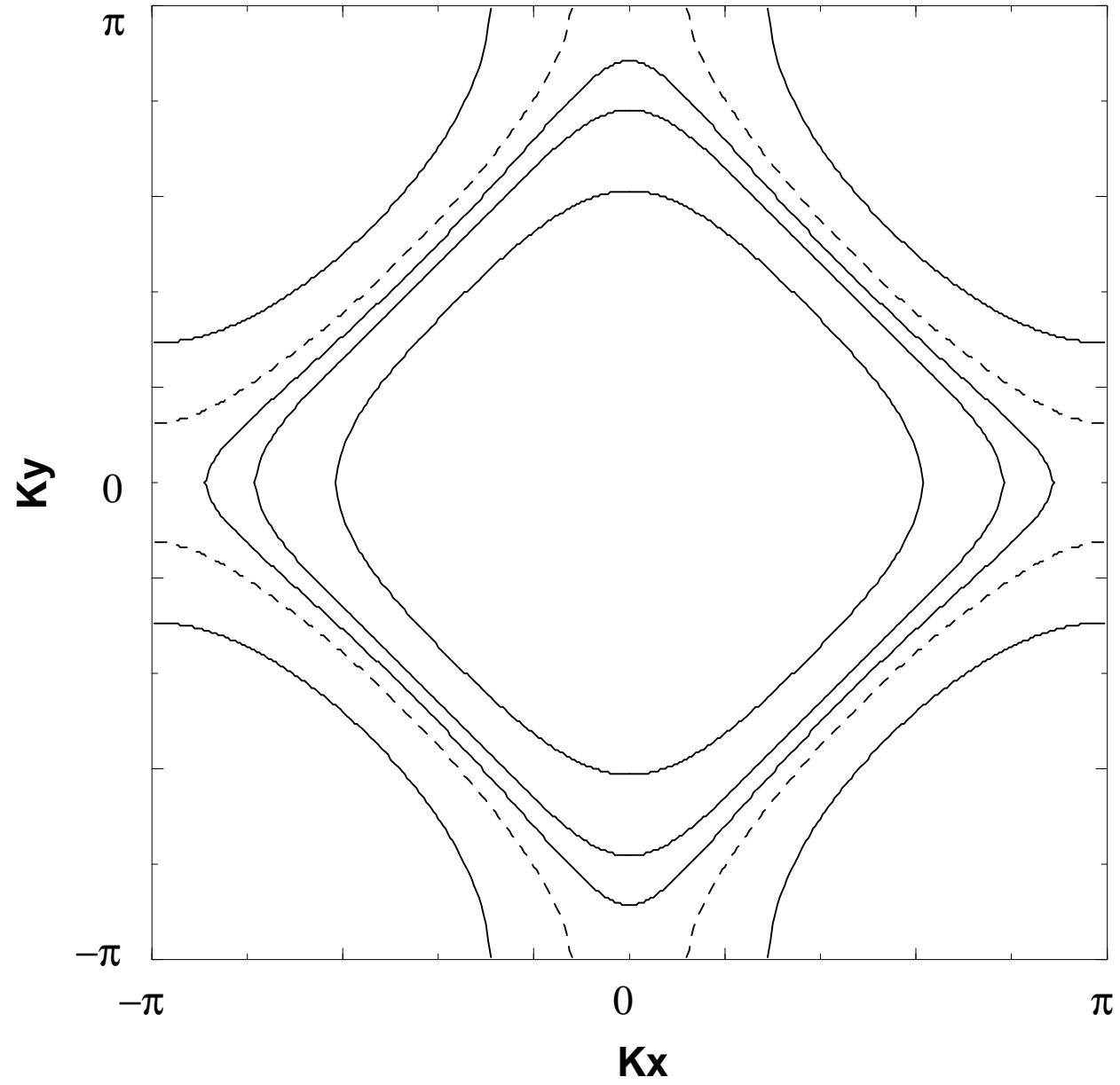


figure4

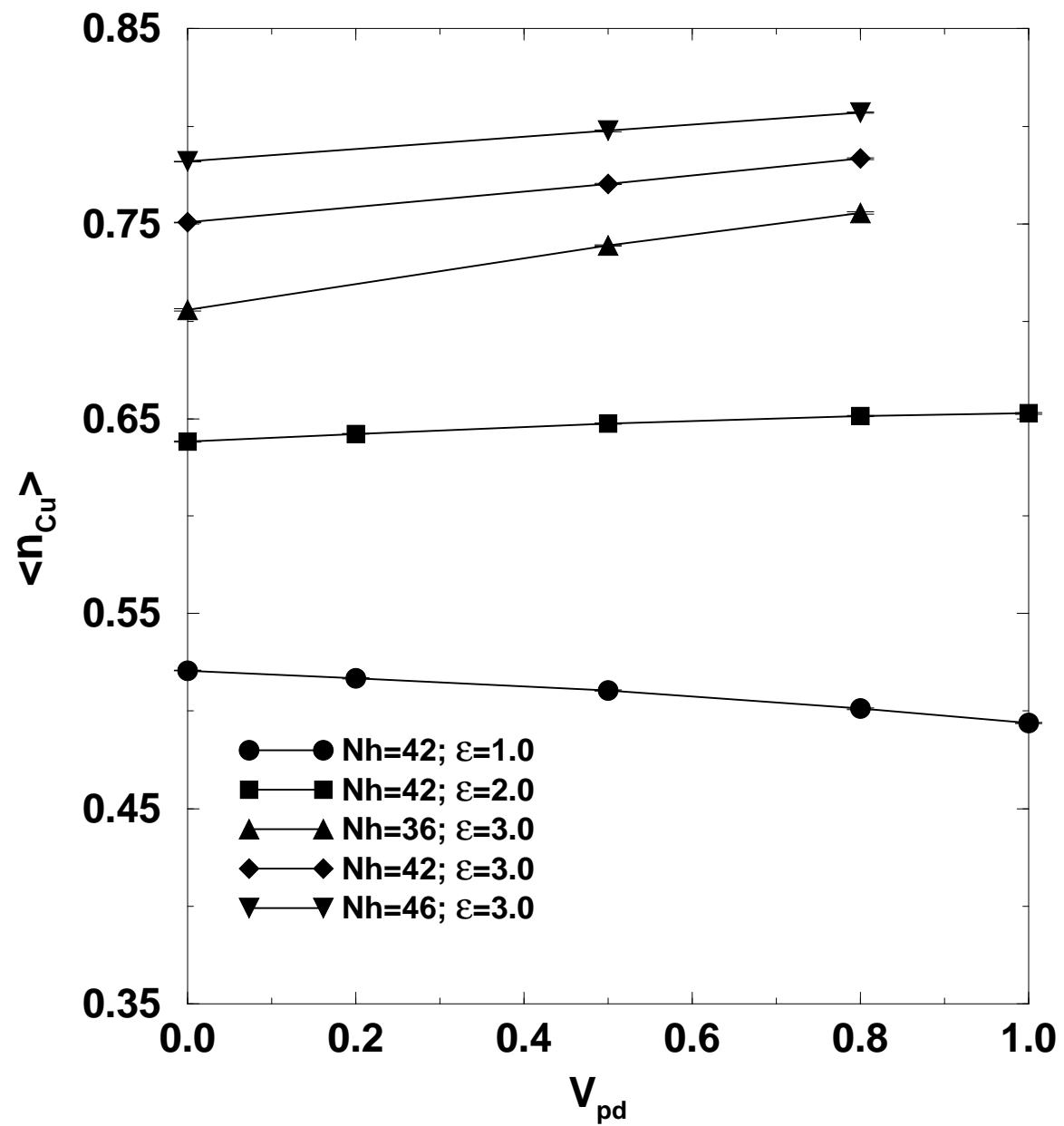


figure5

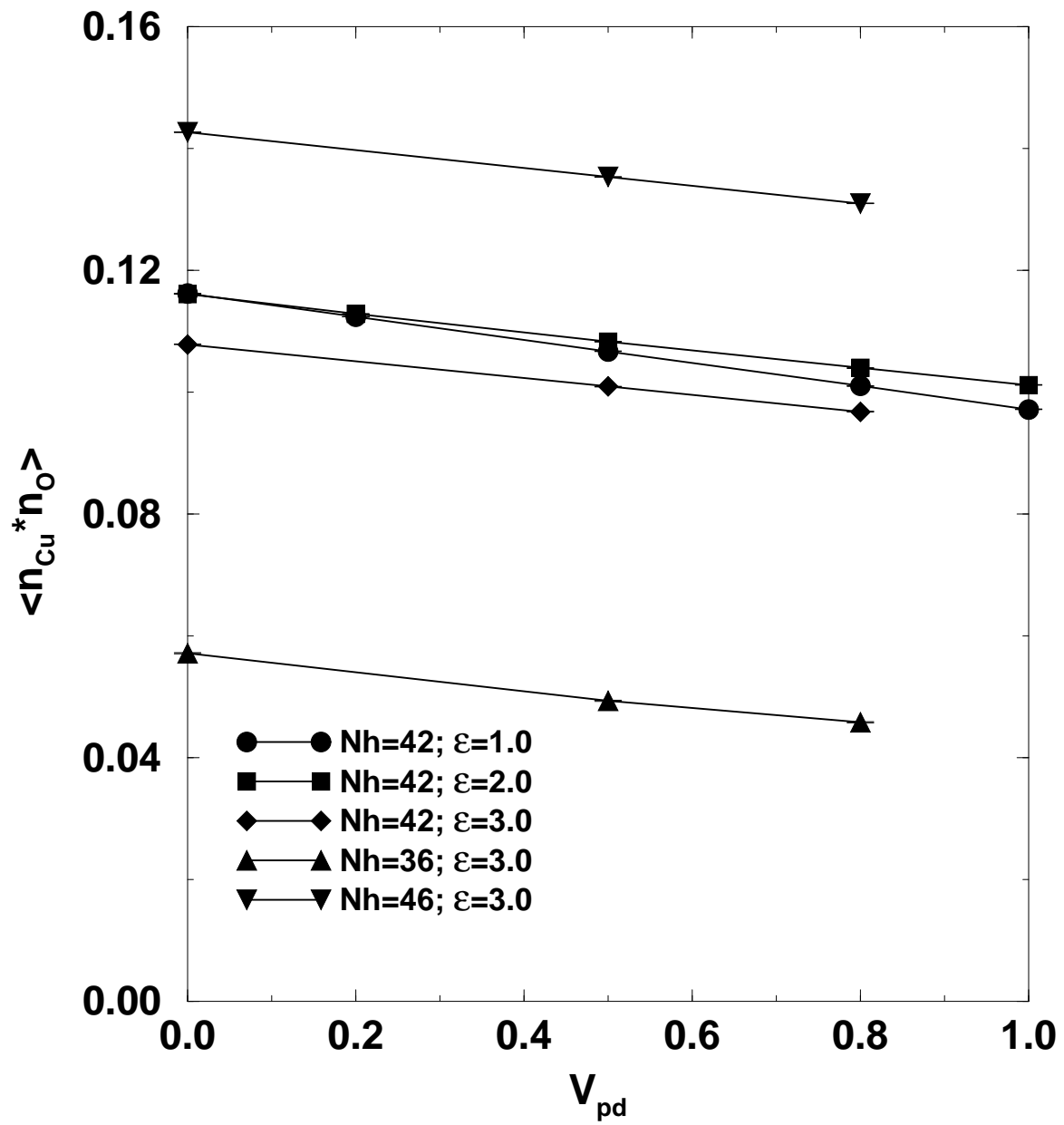


figure6

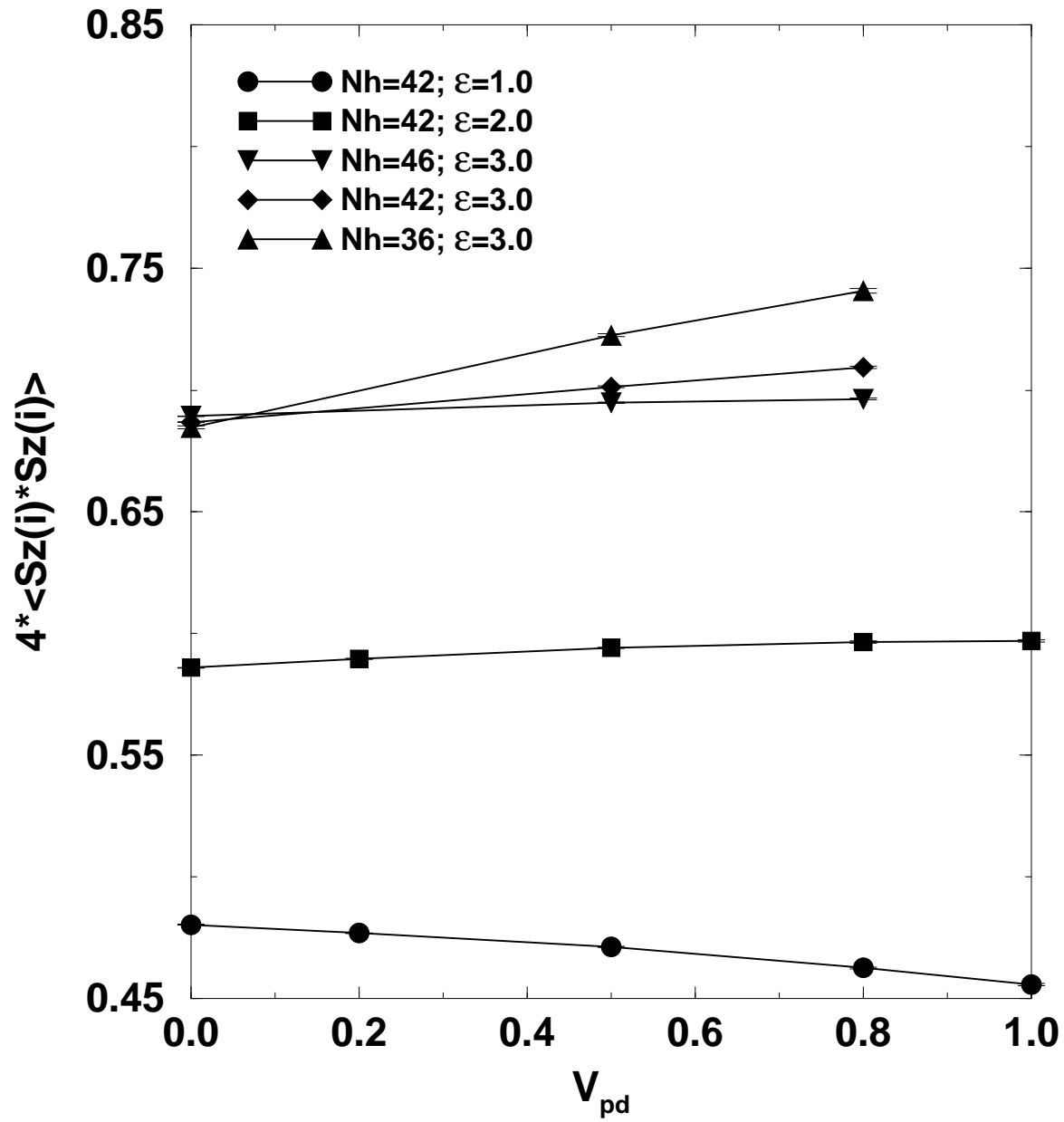


figure7

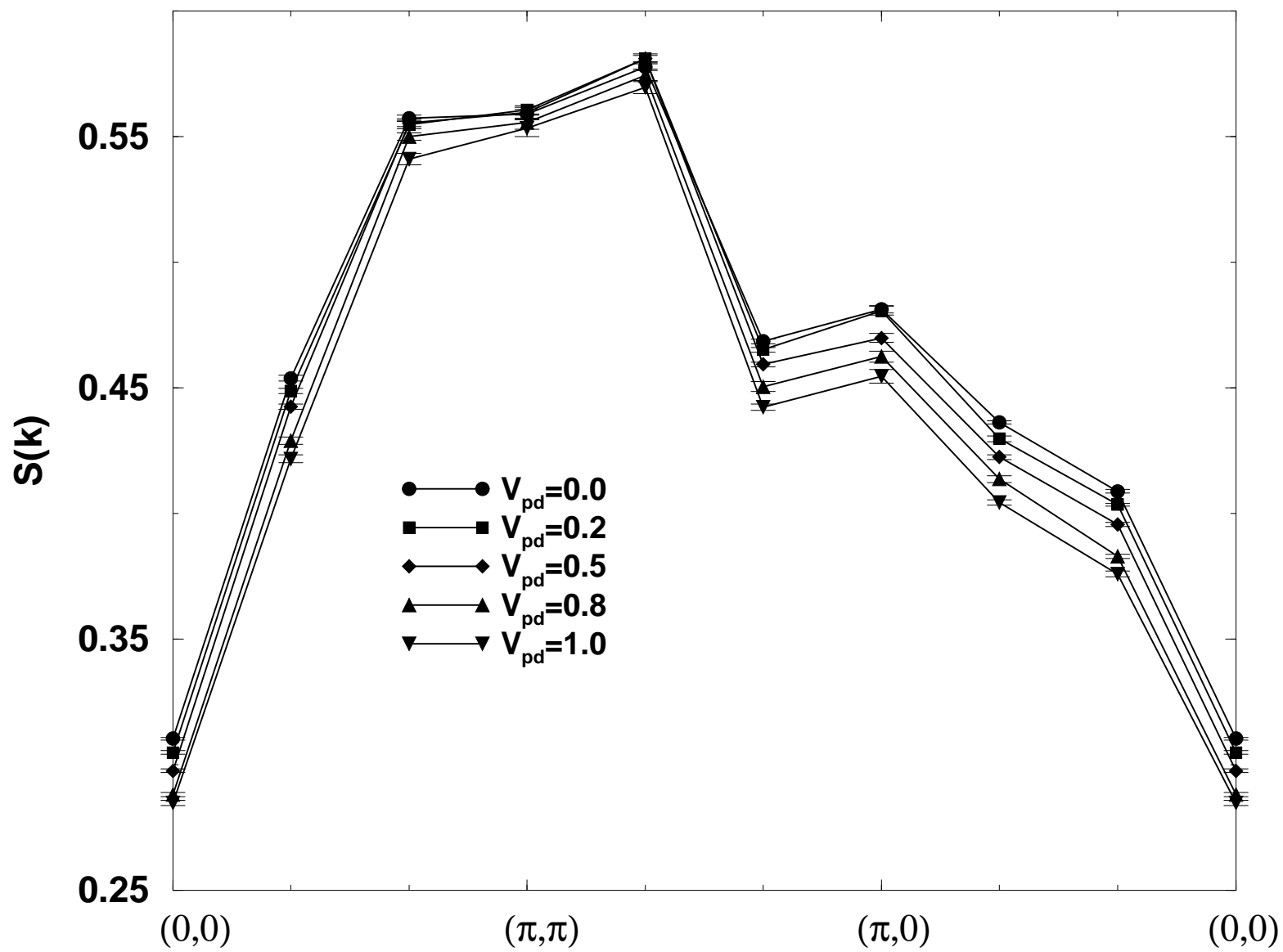


figure8

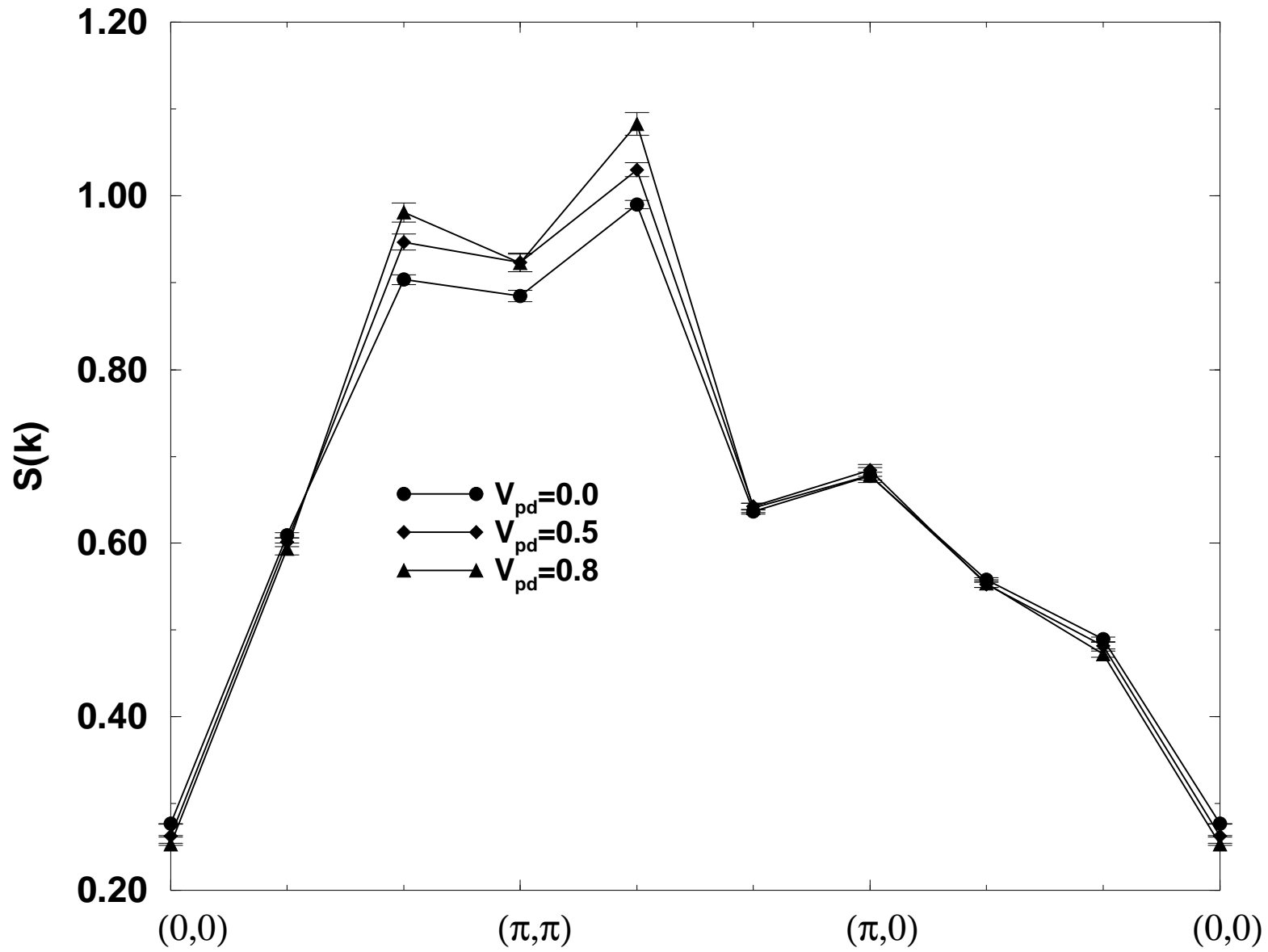


figure9(a) and figure9(b)

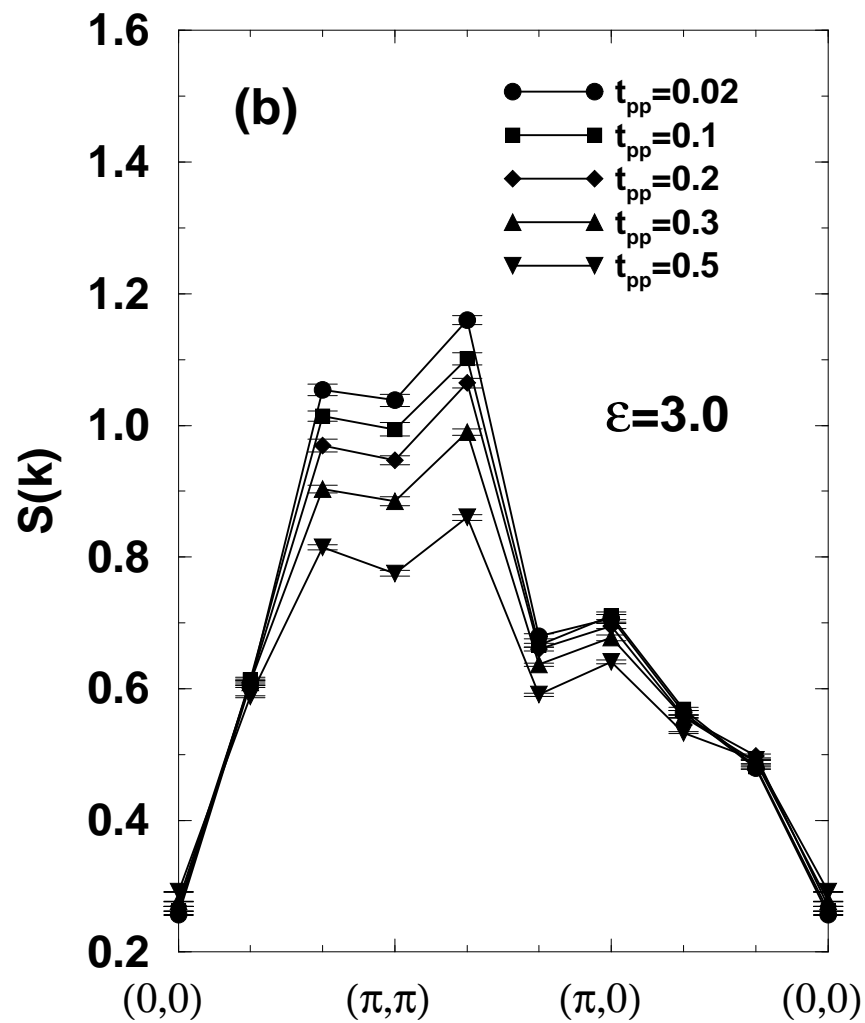
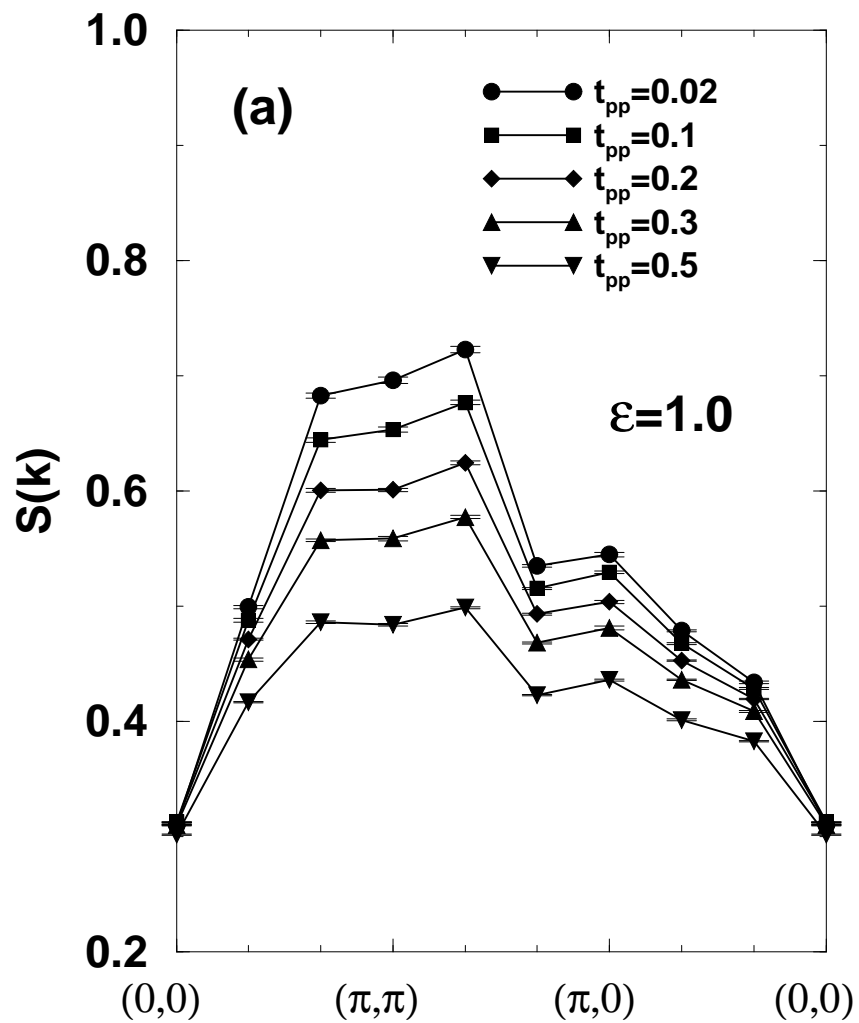


figure10(a) and figure10(b)

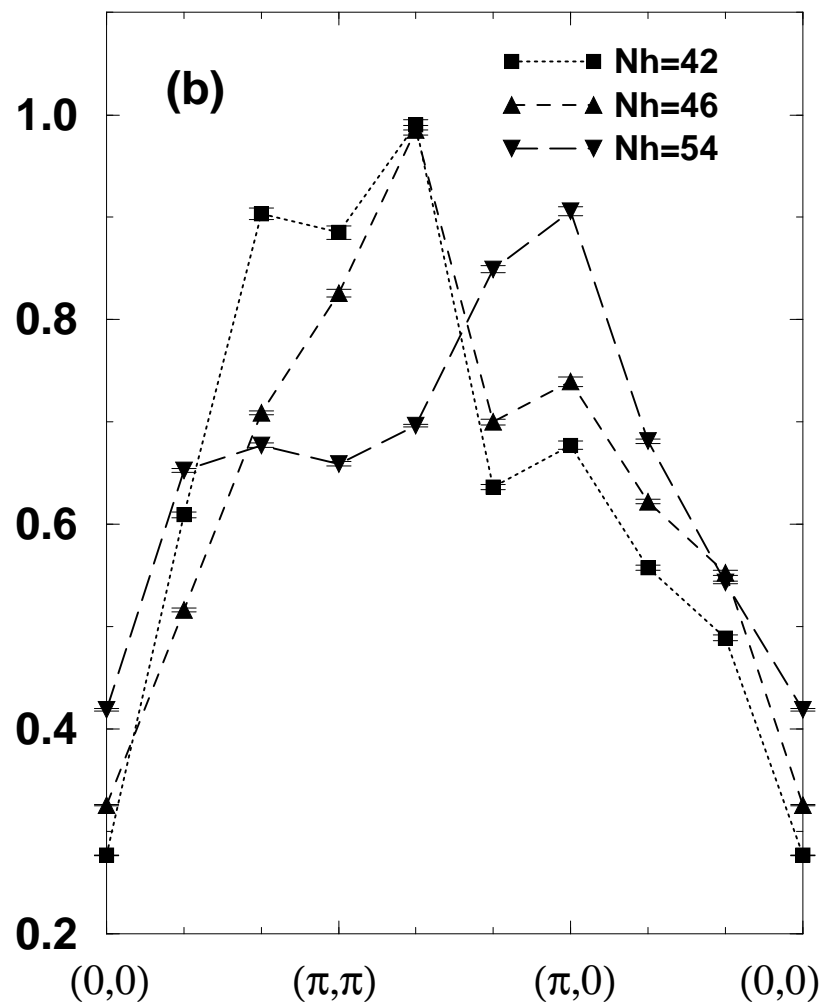
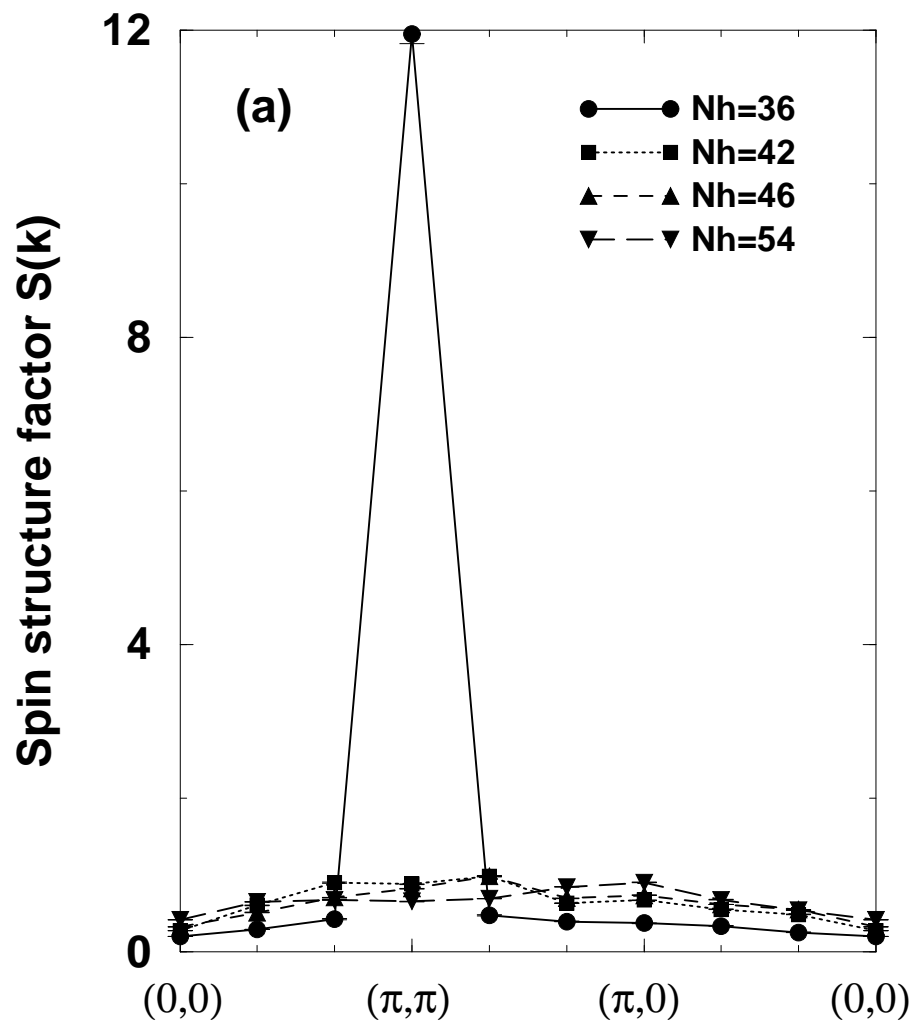


figure11

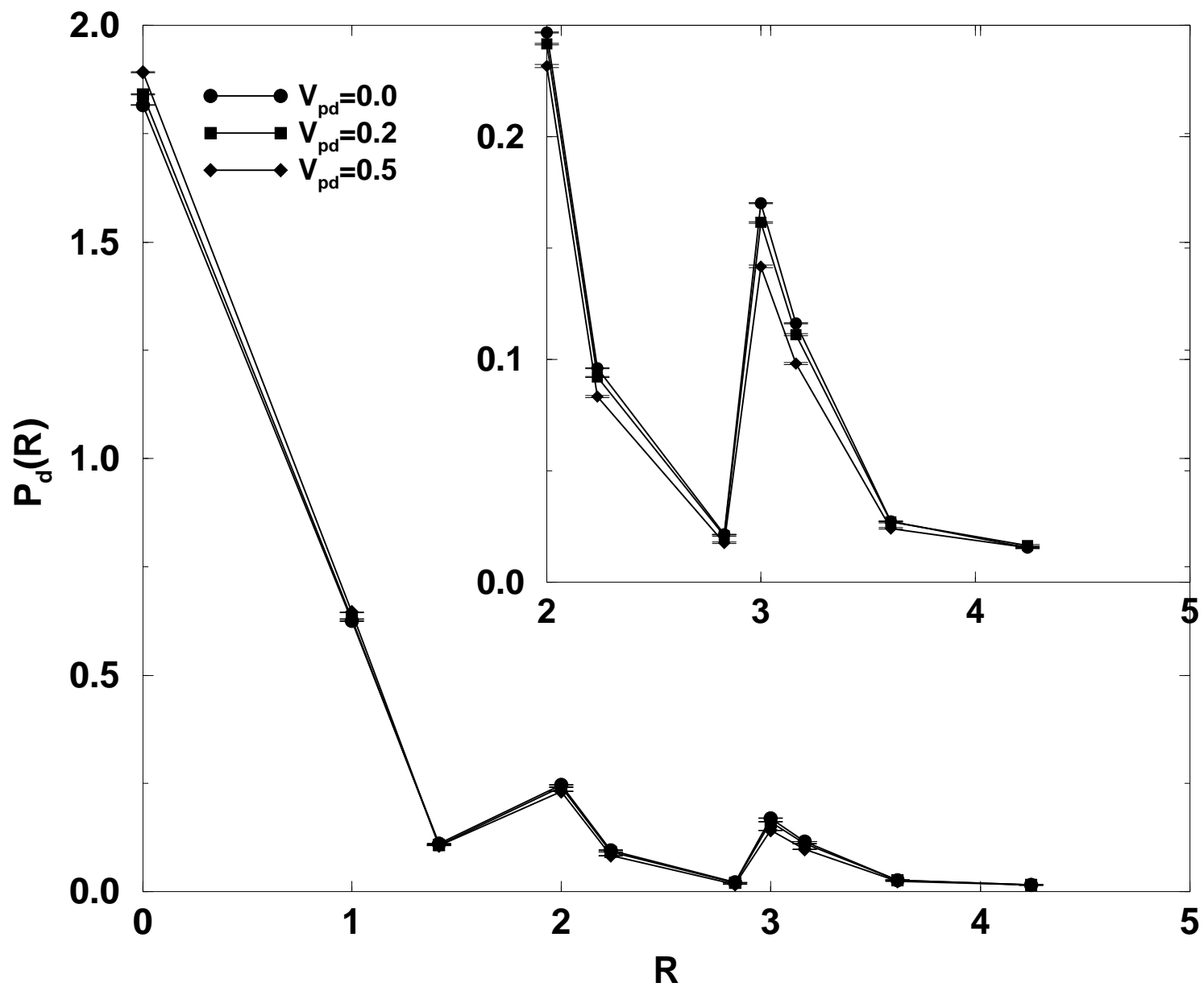


figure12(a) and figure12(b)

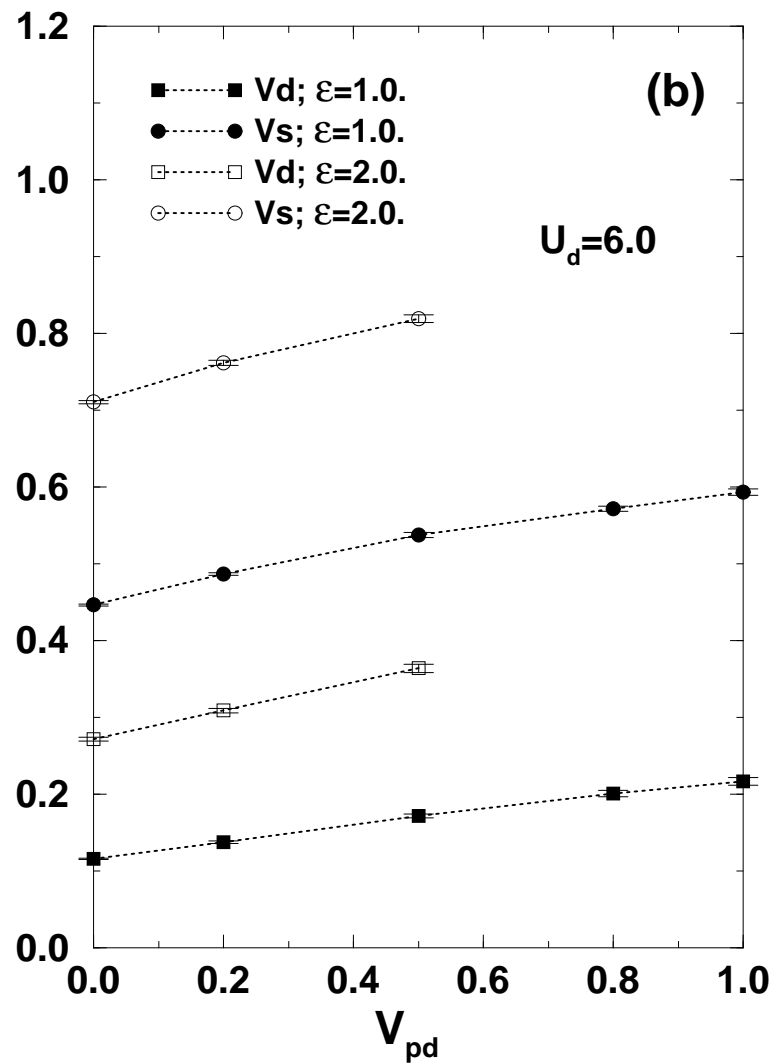
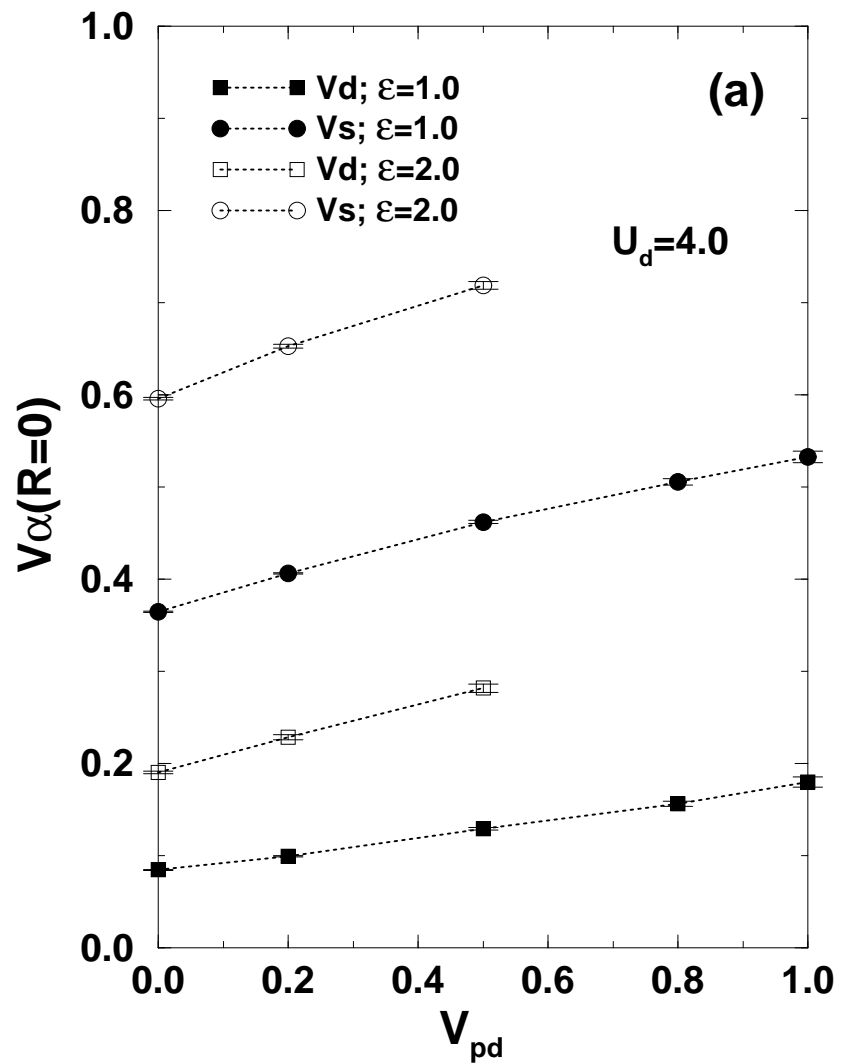


figure13(a) and figure13(b)

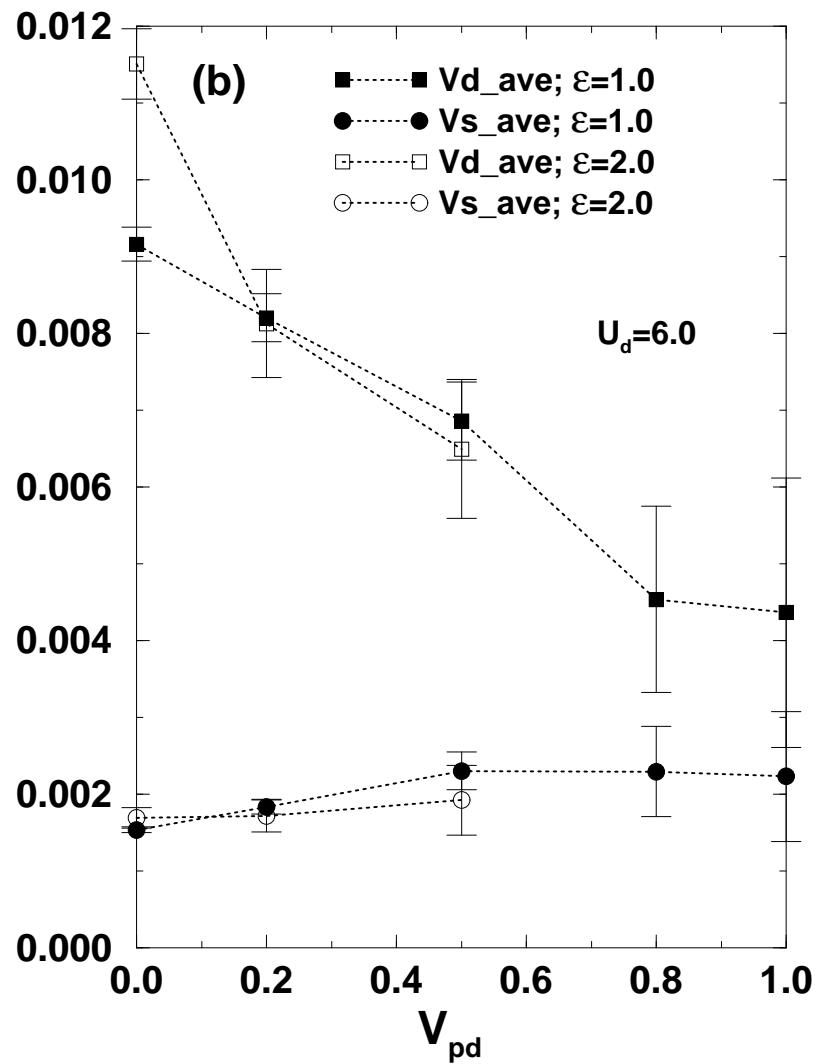
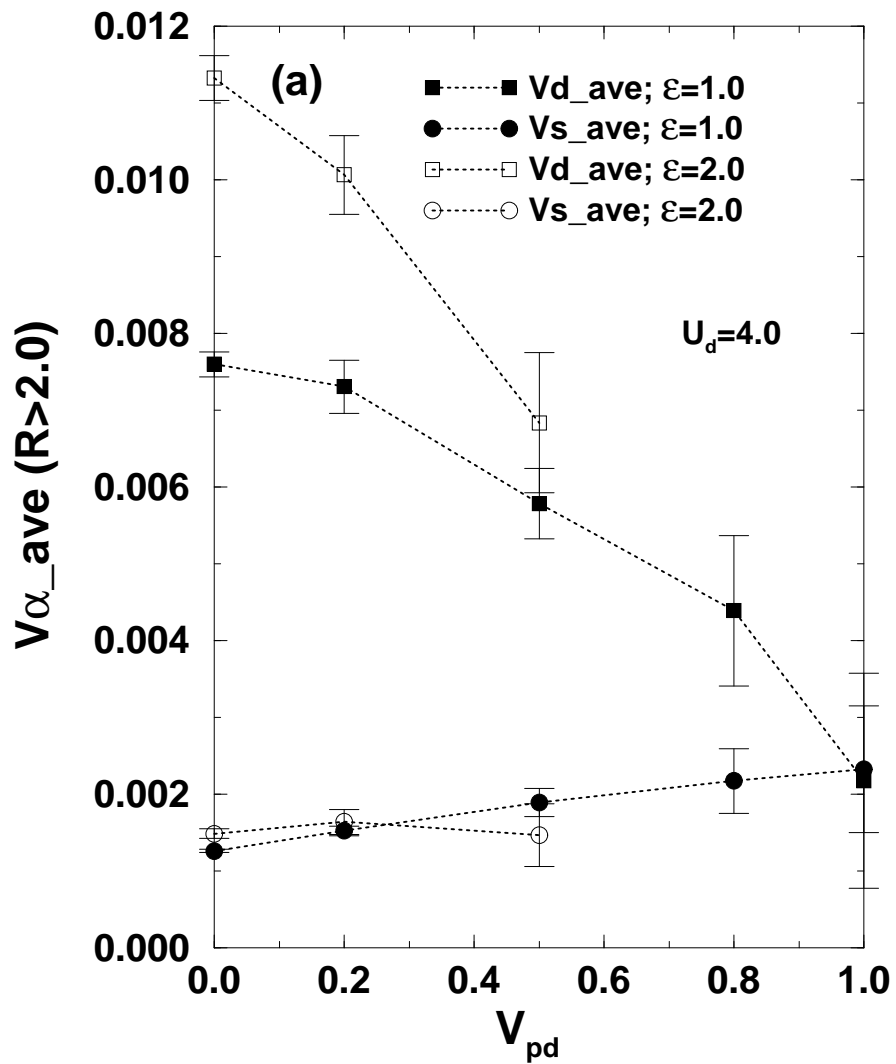


figure14(a) and figure14(b)

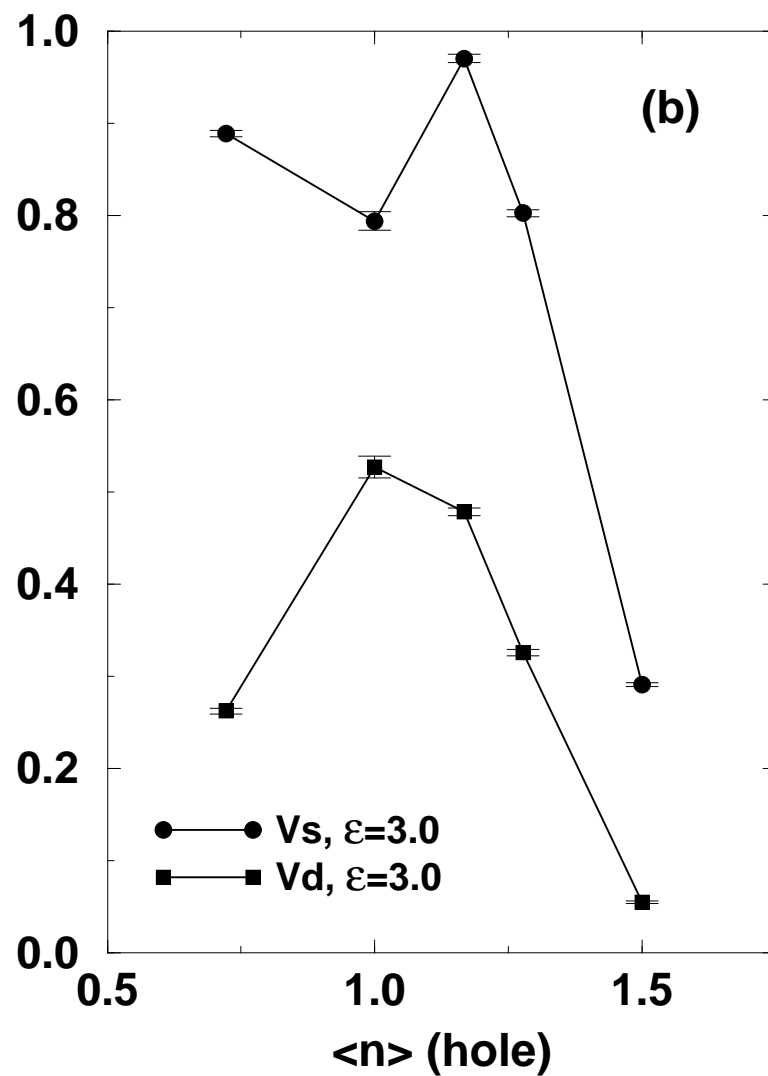
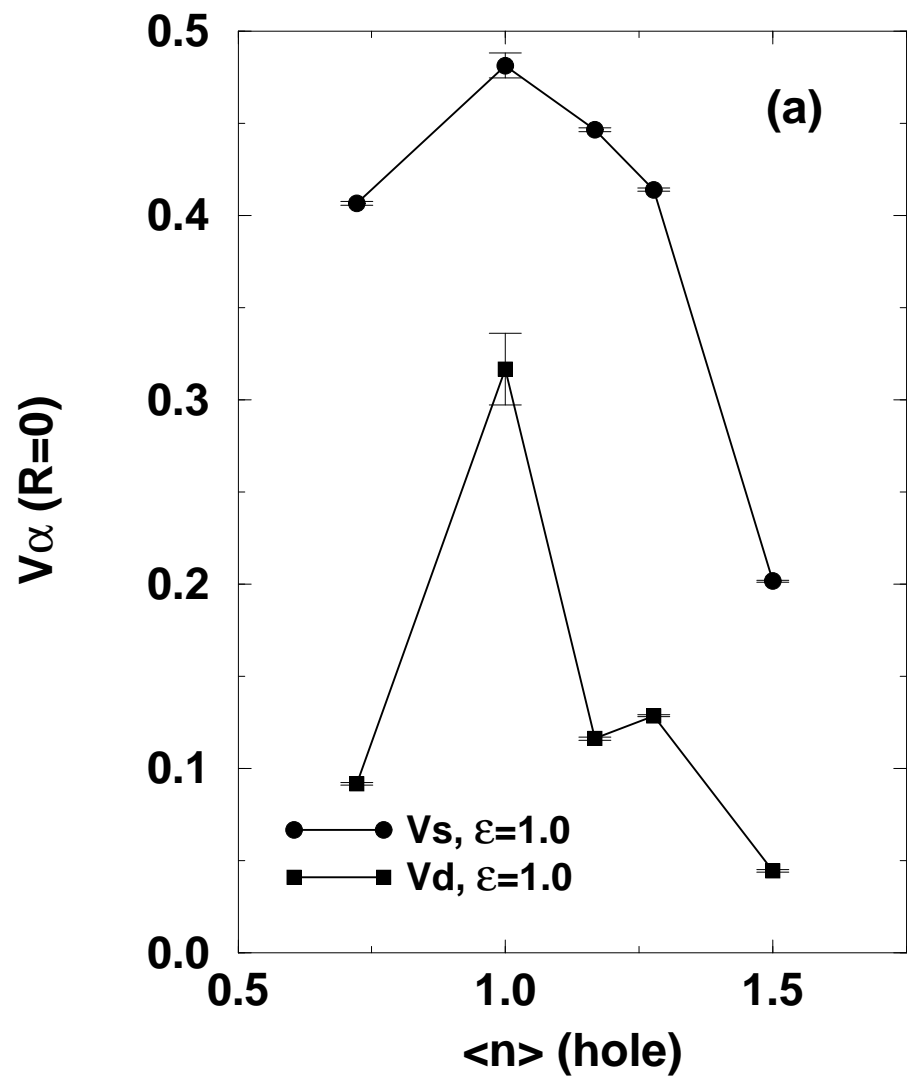


figure15(a) and figure15(b)

